ALCHEMY Jurnal Penelitian Kimia
Laman resmi: https://jurnal.uns.ac.id/alchemy
ISSN 1412-4092
EISSN 2443-4183

Electronic Structure of Vanadium-Doped TiO_2 of Both Anatase and Rutile Based on Density Functional Theory (DFT) Approach

Hari Sutrisno*

Department of Chemistry Education, Faculty of Mathematics and Natural Sciences, Universitas Negeri Yogyakarta, Jl. Colombo No.1, Yogyakarta, Indonesia, 55281

** Corresponding author*

E-mail: sutrisnohari@uny.ac.id

DOI: 10.20961/alchemy.14.1.11374.60-71

Received 2 June 2017, Accepted 10 October 2017, Published online 1 March 2018

ABSTRACT

Study of the theoretical approah to calculate the band structure and density of states (DOS) of vanadium-doped TiO_2 of both anatase and rutile have been done. The first-principle calculations were done using supercell (2x1x1) method. The first-principle calculation of V-doped TiO_2 of both anatase and rutile were analyzed by density-functional theory (DFT) with generalized gradient approximation from Perdew-Burke-Ernzerhof (GGA+PBE), Perdew-Wang's 1991 (GGA+PW91) and local density approximation (LDA) for exchange-correlation functionals. The calculation of electronic structures show that the V-doped TiO_2-anatase with high concentration (7.93%) in 24 atoms are direct- and indirect-gap semiconductor, whereas the V-doped TiO_2-rutile with high concentration (15.79%) in 12 atoms is direct-gap semiconductor. The V-doped TiO_2 of both anatase and rutile produce the intermediate bands in the upper states. Ihe V-doped anatase produces intermediate band, which is 2.05, 2.04, 2.06 eV above the valence band for GGA+PBE, GGA+PW91 and LDA, respectively. Meanwhile the V-doped rutile produces–intermediate band, which is 1.76, 1.82, 1.74 eV above the valence band for GGA+PBE, GGA+PW91 and LDA, respectively.

Keywords: anatase, band-gap DFT, electronic structure, rutile.

INTRODUCTION

Titanium dioxide or titania (TiO_2) is a n-type semiconductor. It has eleven different structure phases (allotrop). In nature, TiO_2 has three kinds of crystal structure: anatase, rutile and brookite. Anatase and rutile are the two most stable forms and are both produced on an industrial scale. Anatase phase is a TiO_2 polymorph which is less stable than rutile phase, but more efficient than rutile for several applications, including photocatalysis (Zhang *et al.*, 2016; Muctuma *et al.*, 2015), antibacterial activity (Galkina *et al.*, 2014; Huang *et al.*, 2000; Maness *et al.*, 1999), and dyesensitized solar cells (Grätzel, 2005; Grätzel, 2004). In all these applications, surface properties are of major importance.

However, such potential applications are seriously limited by the intrinsic wide energy gaps of TiO_2, which confine the advantages of the TiO_2 phases to be viable only under ultraviolet (UV) radiation.

Many attempts have been made to improve the photocatalytic performance of TiO_2 under visible-light irradiation, such as through transition metal (V, Mn, Fe, Cu, Ce, W, Cr, Co, Ag, etc.) (Al-Hartomy, 2014; Chang and Liu, 2014; Yang *et al.,* 2014; Zhang *et al.,* 2013; Tian *et al.,* 2012; Thuy *et al.,* 2012; Liu *et al.,* 2009) and non-metal doping (N, C, S, etc.) (Zhao *et al.,* 2013: Dong *et al.,* 2008; Zhao *et al.,* 2008; Yang *et al.,* 2007), noble metal deposition on TiO_2 surfaces (Ma *et al.,* 2014; Wang *et al.,* 2008), semiconductor coupling (Hoyer and Weller, 1994), inorganic sensitizing (Hu *et al.,* 2006) and organic dye sensitizing (Tan and Wu, 2006). The most promising method to reduce the effective band gap of TiO_2 is through the doping of impurities into the TiO_2 lattice to modify its electronic structure. Especially in recent years, a number of attempts have been made to improve the visible-light absorption of TiO_2 both with transition metal (V, Mn, Fe, Cu, Ce, W, Cr, Co, Ag, etc.) and non-metal dopants (N, C, S, etc.) to modify the electronic structure and improve the photocatalytic reaction efficiency which was strongly influenced by the recombination rate of photo-generated electrons and holes.

Theoretical investigations have also been carried out to study the energy band structures of TiO_2 phases including anatase and rutile. The rutile phase, which is the most stable form of TiO_2, exhibits a direct band structure of 3.0 eV (Grant, 1959), while the band structure of the metastable anatase phase is indirect band structure of 3.2 eV in nature (Tang *et al.,* 1994). Some studies have also been made by several groups to introduce vanadium metal which can improve the photocatalytic activity of TiO_2 and extend its optical absorption to the visible-light region.

Pure TiO_2 is a wide band-gap semiconductor with the O *p* band filled and the Ti-*d* band empty. When a V atom replaces a Ti atom the resulting system is metallic because of the lack of two electrons necessary to fill up the O *p* band (Wang *et al.,* 2014; Peng *et al.,* 2014). Thus, it can be expected that V-incorporation in TiO_2 can result in some unusual optical transitions and the optical absorption in the visible range. Two type of the doping of vanadium in the TiO_2 lattice are substitutional (Islam *et al.,* 2015; Wang *et al.,* 2014) and interstitial (Kokorin *et al.,* 2016). The electronic properties of vanadium-doped rutile TiO_2 are investigated theoretically with a Hartree-Fock/DFT hybrid approach by Islam et al. (2015). They used supercells ($Ti_{16}O_{32}$, $Ti_{32}O_{64}$, and $Ti_{54}O_{108}$) as models of the doped rutile TiO_2. In the present study, we considered substitutional doping of V^{4+} in both anatase and

rutile phases. The electronic properties of V^{4+}-doped TiO_2 of anatase (Ti_7VO_{16}) and rutile (Ti_3VO_8) have been investigated using the (2x1x1) supercell model by using the first-principles calculation based on density-functional theory (DFT). This is essential for a proper understanding of the material itself and also of the processes used for its production on an industrial.

METHODS

All calculations presented are based on density-functional theory (DFT). Kohn-Sham density functional theory calculations are performed with the density functional theory (DFT) using the local density approximation (LDA) (Kohn and Sham, 1965) and generalized gradient approximation (GGA) proposed by Perdew-Burke-Ernzerhof (GGA+PBE) (Perdew *et al.,* 1996), Perdew and Wang's 1991 (GGA+PW91) (Perdew *et al.,* 1992) for the exchange correlation potential. The electronic properties of V-doped TiO_2 of both anatase and rutile phases have been investigated using the (2x1x1) supercell model as implemented within ADF-BAND package of version 2014.10 (SCM, 2014). The substitutional method has been taken into account in this paper. The V atoms are used to substitute Ti atom in TiO_2, because atom radius of V are larger than the O atom. The doped TiO_2 systems form the configurations of V^{4+}-doped TiO_2 of anatase (Ti_7VO_{16}) and rutile (Ti_3VO_8).

The unit cell of TiO_2 in anatase, rutile and (2x1x1) supercell model considered in this study are shown in Figure 1a, 1b, 2a, and 2b. The ideal anatase TiO_2 has a tetragonal structure with the space group $I4_1/amd$, which contains four titanium atoms and eight oxygen atoms in unit cell. The cell parameters are $a = b = 3.785$ Å and $c = 9.514$ Å (Weirich *et al.,* 2000). The structure of anatase can be described in terms of chains of TiO_2 octahedra. Each Ti^{4+} ion is surrounded by an octahedron of six O^{2-} ions. Our model consists of two unit cells stacked along the *a*-axes, where one Ti atom is substituted by a 3*d* transition V atom. The (2×1×1) supercell model of V-doped anatase phase contains 24 atoms, in this way the structure of Ti_7VO_{16} is obtained. The atomic percentage of the impurity was found to be 7.93 at% (Figure 1b).

The rutile structure belongs to the tetragonal crystal system (space group $P4_2/mnm$), and the lattice parameters are $a = b = 4.594$ Å and $c = 2.958$ Å (Swope *et al.*, 1995). The (2×1×1) supercell model of V-doped rutile phase is composed of 12 atoms, which

correspond to $Ti_{(1-x)}V_xO_2$ (x = 0.25), in this way, the structure of Ti_3VO_8 is obtained. The atomic percentage of the impurity was found to be 15.79 at % (Figure 2b).

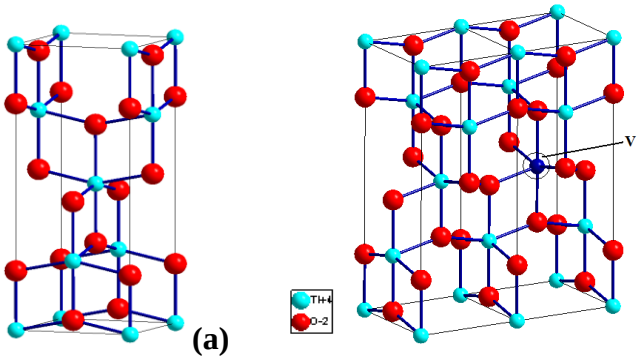

Figure 1. Models for calculation, (a) unit cell of anatase and (b) structure of (2x1x1) supercell model of V-doped anatase containing 24 atoms (Ti_7VO_{16})

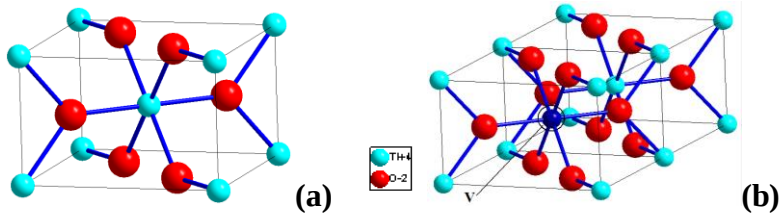

Figure 2. Models for calculation, (a) unit cell of rutile and (b) structure of (2x1x1) supercell model of V-doped rutile containing 12 atoms (Ti_3VO_8)

RESULTS

Band Structure and Density of State (DOS) of V-doped Anatase

The V-doped anatase band structure along the direction of the brillouin zone high symmetry point is as in Figure 3. Figure 3 shows the top of valence band which approximately locates near the k-point = 1, and the bottom of the conduction band which locates at the k-point = 1 or k-point = 16. This means that TiO_2 with V-doped anatase TiO_2 structure is direct and indirect-gap semiconductor.

Figure 4 gives the partial and total density of states (DOS) of V-doped anatase within GGA+PBE, GGA+PW91 and LDA using the (2x1x1) supercell method. The valence band of V-doped TiO_2-anatase mainly consists of the 2*p*, 2*s* states of O and 3*d* states of V and Ti. The upper valence bands show a strong hybridization between 2*p* orbitals from O atoms and 3*d* orbitals from V and Ti atoms. The top of the valence bands was dominated by the O 2*p* orbitals, while the conduction bands, especially the bottom, contain significant contributions from the V 3*d* and Ti 3*d* orbitals. It is obvious from anatase model in Figure 1b that the doped V 3*d* orbitals substantially contributed to the valence bands and the impurity bands. The Ti 3*d* and V 3*d* states give rise to some bands in the energy range from 4.00 to 11.00 eV. The lowest conduction band is dominated by V 3*d*

states. Meanwhile, the hybridization among the V 3*d*, Ti 3*d* and O 2*p* levels at the valence band can be observed as in Figure 4. In the uppermost valence band, the O 2*p* states are predominantly found between -2.50 to 2.50 eV, while the O 2*s* states appear in the range from -15.00 to -13.00 eV.

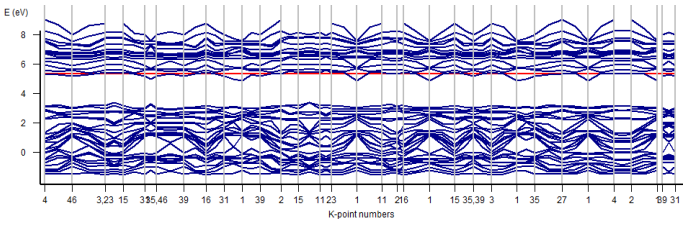

GGA+PBE

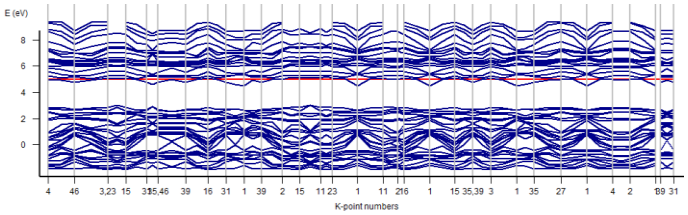

GGA+PW91

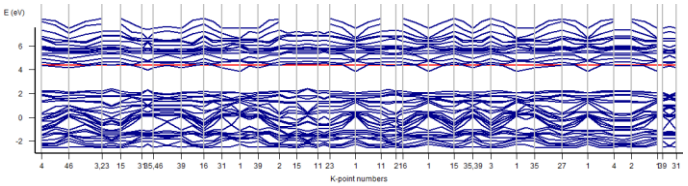

LDA

Figure 3. The band structure of V-doped anatase within GGA+PBE, GGA+PW91 and LDA using the (2x1x1) supercell method.

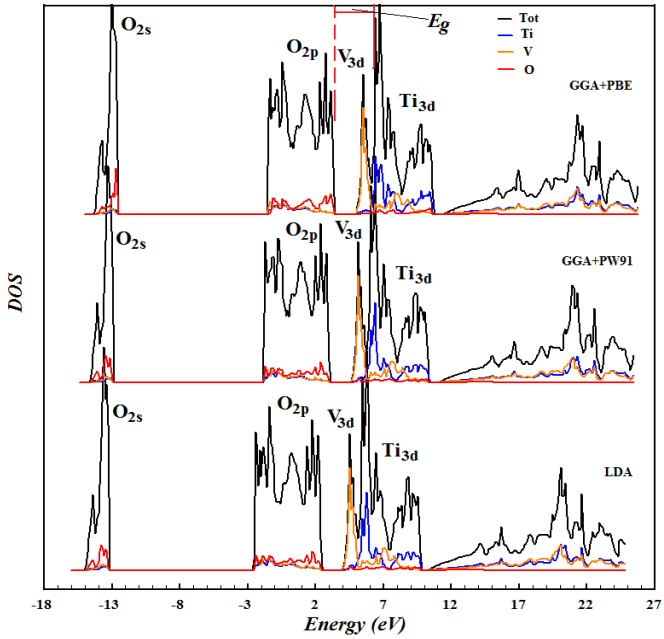

Figure 4. The corresponding total-density of state (t-DOS, *black line*) and partial-density of state (p-DOS, *blue*, *yellow and red line*) of V-doped anatase within GGA+PBE, GGA+PW91 and LDA using the (2x1x1) supercell method.

The V 3*d* states in V-doped TiO_2-anatase have been observed in the energy range from 2.00 to 3.00, 2.50 to 3.50 and 2.75 to 3.75 eV. The O 2*s* states have slightly shifted to low energy range. V-incorporation atom induces the increasing *p* states in the top of valence band. The valence band mainly consists of the 2*p*, 2*s* states of O and 3*d* states of V and Ti. In this early calculations, the V-doped anatase with 7.93% in 24 atoms produced upper states, and it was 2.05, 2.04, 2.06 eV above the valence band and 0.48, 0.54 and 0.47 eV below the conduction band for GGA+PBE, GGA+PW91 and LDA, respectively (Figure 5), which are suitable with the experimental value of V-doped TiO_2 -anatase with high concentration (4.17%) in 24 atoms, and it was 1.82 eV above the valence band (Wang *et al.*, 2014). The band gaps of the V-doped anatase from this research have a much smaller value than the band gap un-doped TiO_2 (anatase) calculation using LDA method that is equal to 2.59 eV (Sutrisno and Sunarto, 2014).

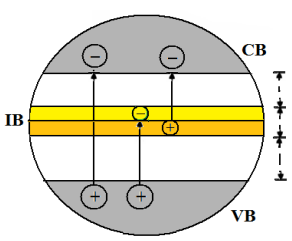

GGA+ PBE	GGA+ PW91	LDA
0.48 eV	0.54 eV	0.47 eV
0.56 eV	0.57 eV	0.54 eV
2.05 eV	2.04 eV	2.06 eV
Eg (O_{2p} to Ti_{3d})		
3.09 eV	3.20 eV	3.14 eV

Figure 5. The Intermediate band of V-doped anatase with 7.93% in 24 atoms produced upper states within GGA+PBE, GGA+PW91 and LDA using the (2x1x1) supercell method.

In the uppermost valence band, O 2*p* states are predominantly found between -4.50 and 1.00 eV, while O 2*s* states appear in the range from -15.0 to -13.0 eV. The V 3*d* states give rise to some bands in the energy range from 4.00 to 5.00 eV, meanwhile the Ti 3*d* states are predominantly found between 5.00 to 10.00 eV. As Wang *et al.* (2014) clarified for V-doped TiO_2-anatase, the D_{4h} symmetry caused the three-fold degenerate t_{2g} ($3d_{xy}$, $3d_{xz}$, and $3d_{yz}$) and two-fold degenerate e_g ($3d_x2_{-y}2$ and $3d_z2$) of a transition metal cation to further split; the t_{2g} split into a two-fold degenerate levels of both $3d_{yz}$ and $3d_{xz}$ and a level of $3d_{xy}$ while the e_g split into two levels of $3d_x2_{-y}2$ and $3d_z2$.

Density of State (DOS) and Band Structure of V-doped Rutile

Band structure and density of states (DOS) V-doped TiO_2-rutile within GGA+PBE, GGA+PW91 and LDA using (2x1x1) supercell method are performed in the configuration of Ti_3VO_8, which is presented in Figure 6 and **7**, respectively. In Figure 6, the top of valence band approximately locates near the k-point = 1 and the bottom of the conduction band locates at the k-point = 1; this means that V-doped rutile structure is a direct-gap semiconductor. The valence band of V-doped TiO_2-rutile mainly consists of the 2*p*, 2*s*

states of O and 3*d* states of V and Ti. The upper valence bands showed a strong hybridization between 2*p* orbitals from O atoms and 3*d* orbitals from V and Ti atoms.

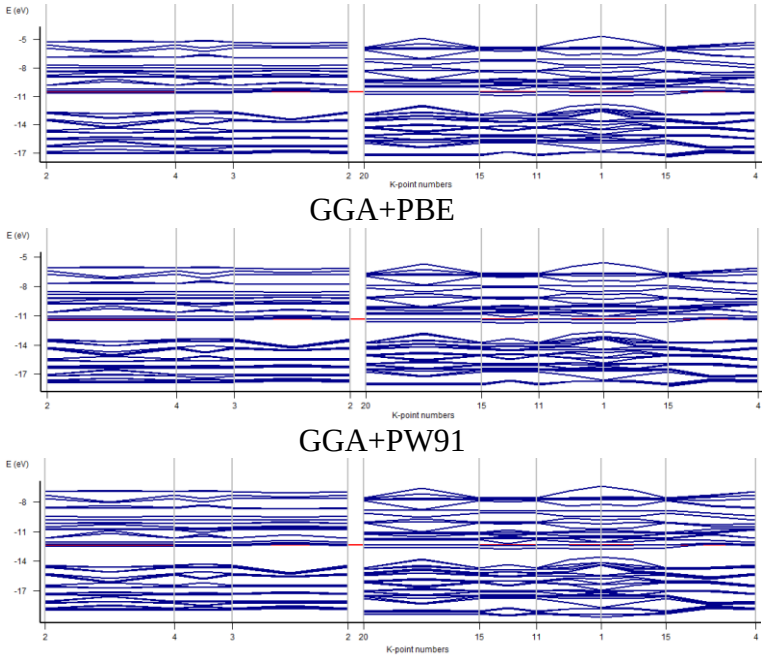

Figure 6. The band structure of V-doped rutile within GGA+PBE, GGA+PW91 and LDA using the (2x1x1) supercell method.

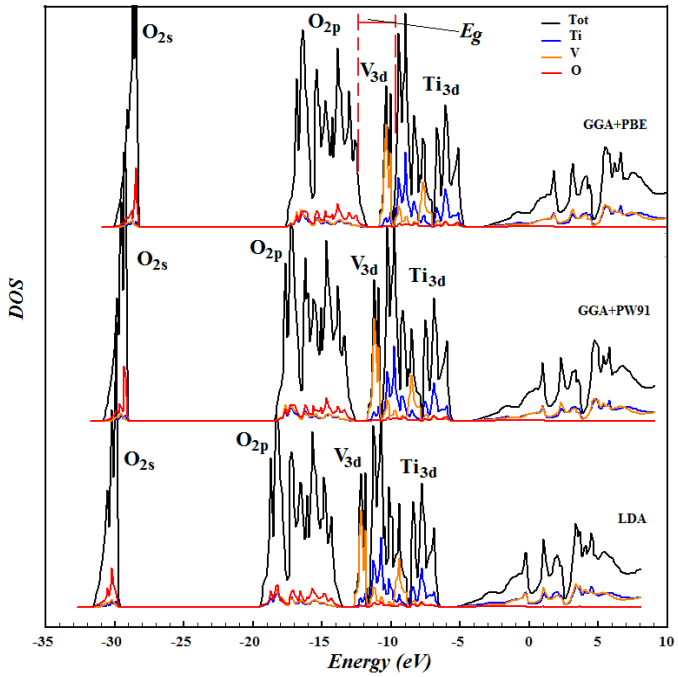

Figure 7. The corresponding total-density of state (t-DOS, *black line*) and partial-density of state (p-DOS, *blue, yellow and red lines*) of V-doped rutile within GGA+PBE, GGA+PW91 and LDA using the (2x1x1) supercell method.

The V-doping can induce the upper states in band gap, which are mainly composed of the 3*d* and 2*p* electronic states. From the results of DOS of V atoms in Figure 7, the 3*d* electronic states are mainly attributed to the V, while the *p* electronic states are due to the

O 2*p* states. These results are consistent with the previous experimental and theoretical results (Prasai *et al.*, 2012; Mo *et al.*, 1995). In this early calculations, the V-doped rutile with 15.79% in 12 atoms produced upper states, and it was 1.76, 1.82, 1.74 eV above the valence band and 0.41, 0.39, 0.41 eV below the conduction band for GGA+PBE, GGA+PW91 and LDA, respectively (Figure 8). These midgap electronic states may induce some visible optical transition. Meanwhile, the *p* and *d* states have been observed in the energy range of 7-9 eV at the bottom of valence band due to the doping of V. These *p* and *d* states are similar to the midgap states. To the V-doped TiO_2-rutile, it is observed that the 3*d* states of Ti mainly appear at the valence band, particularly, dominated at the top and bottom of valence band. Thus, the enhanced *d* states of V-doped TiO_2-rutile at the uppermost valence band are due to the V-dopant, which is consistent with the previous theoretical results. Even in the high concentration doping (Ti_3VO_8) system, the V 3*d* states also located above the valence band using GGA+PBE, GGA+PW91 and LDA method. The increasing *d* electronic states of V-doped TiO_2-rutile at the uppermost valence band lead to the band gap narrowing. The valence band mainly consists of the 2*p*, 2*s* states of O and 3*d* states of V and Ti. In the uppermost valence band, O 2*p* states were predominantly found between -19.00 and -13.00 eV, while O 2*s* states appear in the range from -32.00 to -28.00 eV. The V 3*d* states give rise to some bands in the energy range from -13.00 to -12.00 eV, meanwhile The Ti 3*d* states were predominantly found between -9.00 to -5.00 eV. The calculated minimum band gaps of GGA+PBE, GGA+PW91 and LDA are about 1.74, 1.79 and 1.78, eV respectively, which are less than the experimental value of un-doped TiO_2-rutile of 3.00 eV (Grant, 1959). The band gaps of the V-doped anatase from this research have smaller value than the band gap of un-doped TiO_2 (rutile) generated from the calculated using LDA method of 1.67 eV (Sutrisno and Sunarto, 2014).

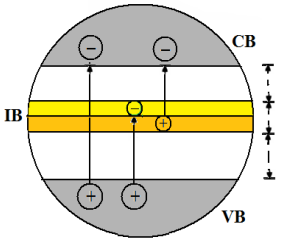

GGA+ PBE	GGA+ PW91	LDA
0.41 eV	0.39 eV	0.41 eV
0.59 eV	0.58 eV	0.61 eV
1.74 eV	1.82 eV	1.76 eV
Eg (O_{2p} to Ti_{3d})		
2.74 eV	2.79 eV	2.78 eV

Figure 8. The Intermediate band of V-doped rutile with 15.79% in 12 atoms produced upper states within GGA+PBE, GGA+PW91 and LDA using the (2x1x1) supercell method.

CONCLUSION

The first-principle calculation of V-doped TiO_2 of both anatase and rutile were analyzed by using density-functional theory (DFT) with generalized gradient approximation from Perdew-Burke-Ernzerhof (GGA+PBE), Perdew-Wang's 1991 (GGA+PW91) and local density approximation (LDA) for exchange-correlation functionals. The calculation of electronic structures show that the V-doped TiO_2-anatase with high concentration (7.93%) in 24 atoms are direct- and indirect-gap semiconductor, whereas the V-doped TiO_2-rutile with high concentration (15.79%) in 12 atoms is direct-gap semiconductor. The V-doped TiO_2 of both anatase and rutile produce the intermediate bands in the upper states of band gap. The calculated band gaps of V-doped TiO_2-anatase from GGA+PBE, GGA+PW91 and LDA are 2.05, 2.04, 2.06 eV above the valence band and 0.48, 0.54 and 0.47 eV below the conduction band, respectively. The V-doped TiO_2-rutile produces intermediate band, which are 1.76, 1.82, 1.74 eV above the valence band and 0.41, 0.39, 0.41 eV below the conduction band for GGA+PBE, GGA+PW91 and LDA, respectively.

ACKNOWLEDGEMENTS

The author would like to thank the Rector of Yogyakarta State University, Yogyakarta, for his support of publishing this article.

REFERENCES

Al-Hartomy, O.A., 2014. Synthesis, Characterization, Photocatalytic and Photo-Voltaic Performance of Ag-Doped TiO_2 Load on The Pt-Carbon Spheres. *Material Science in Semiconductor Processing* 27, 71-78.

Chang, S. M., and Liu, W. S., 2014, The Roles of Surface-Doped Metal Ions (V, Mn, Fe, Cu, Ce, and W) in the Interfacial Behavior of TiO_2 Photocatalysts. *Applied Catalysis B: Environmental* 156-157, 466-475.

Dong, F., Zhao, W., and Wu, Z., 2008. Characterization and Photocatalytic Activities of C, N and S Co-Doped TiO_2 with 1D Nano-Structure Prepared by The Nano-Confinement Effect. *Nanotechnology* 19, 365607-365617.

Galkina, O. L., Sycheva, A., Blagodatskiy, A., Kaptay, G., Katanaev, V. L., Seisenbaeva, G. A., Kessler, V. G., and Agafonov. A.V., 2014, The Sol-Gel Synthesis of Cotton/TiO_2 Composites and Their Antibacterial Properties. *Surface and Coatings Technology* 253, 171-179.

Grant F. A., 1959, Properties of Rutile (Titanium Dioxide). *Review Modern Physics* 31, 646-650.

Grätzel, M., 2004. Conversion of Sunlight to Electric Power by Nanocrystalline Dye-Sensitized Solar Cells. *Journal of Photochemistry and Photobiology A: Chemistry* 164, 3-14.

Grätzel, M., 2005. Solar Energy Conversion by Dye-Sensitized Photovoltaic Cells. *Inorganic Chemistry* 44, 6841-6851.

Hoyer, P and Weller, H., 1994. Particle Size and pH Effects on The Sensitization of Nanoporous Titanium Dioxide Electrodes by Q-Sized Silver Sulfide. *Chemistry Physics Letters* 224(1-2), 75-80.

Hu, C., Hu, X., Wang, L., Qu, H., and Wang, A., 2006. Visible-Light Induced Photocatalytic Degradation of Azodys in Aqueous AgI/TiO_2 Dispersion. *Environmental Science and Technology* 40, 7903-7907.

Huang, Z., Maness, P. C., Blake, D. M., Wolfrum, E. J., Smolinski, S. and Jacoby, W. A., 2000. Bactericidal Mode of Titanium Dioxide Photocatalysis. *Journal of Photochemistry and Photobiology A: Chemistry* 130, 163-170.

Islam, M. M., Bredow, T. and Gerson. A. 2015. Electronic Properties of Vanadium-Doped TiO_2. *Chemical Physics and Physical Chemistry* 12, 3467-3473.

Kohn, W., and Sham, L. J., 1965. Self Consistent Equations Including Exchange and Correlation Effects. *Physical Review B* 140, A1133- A1137.

Kokorin, I., Sukhanov, A., Gromov, O. I., Arakelyan, V. M., Aroutiounian, V. M., and Voronkova, V. K. 2016. EPR Study of TiO_2 (Rutile) Doped with Vanadium. *Applied Magnetic Resonance* 47(5), 479-485.

Liu, B., Wang, X., Cai, G., Wen, L., Song, Y., and Zhao, X., 2009. Low Temperature Fabrication of V-Doped TiO_2 Nanoparticles, Structure and Photo-Catalytic Studies. *Journal of Hazardous Materials* 169, 1112-1118.

Ma, J., Guo, X., Zhang, Y., and Ge, H., 2014. Catalytic Performance of TiO_2@Ag Composites Prepared by Modified Photo-Deposition Method. *Chemical Engineering Journal* 258, 247-253.

Maness, P. C., Smolinski, S., Blake, D. M., Huang, Z., Wolfrum, E. J., and Jacoby, W. A., 1999. Bactericidal Activity of Photocatalytic TiO_2 Reaction, Toward and Undersding of Its Killing Mechanism. *Applied and Environmental Microbiology* 65(9), 4094-4098.

Mo, S. D. and Ching, W. Y., 1995. Electronic and Optical Properties of Three Phases of Titanium Dioxide, Rutile, Anatase, and Brookite. *Physical Review B* 51, 13023-13032.

Muctuma, B. K., Shao, G. N., Kim, W. D., and Kim, H. T., 2015. Sol-Gel Synthesis of Mesoporous Anatase–Brookite and Anatase-Brookite-Rutile TiO_2 Nanoparticles and Their photocatalytic Properties. *Journal of Colloid Interface Science* 442, 1-7.

Peng, L. P., Xu, L., and Xia, Z. C. 2014, Study The High Photocatalytic Activity of Vanadium and Phosphorus Co-Doped TiO_2 from Experiment and DFT Calculations. *Computational Materials Science* 83, 309-317.

Perdew, J. P., Burke, K., and Ernzerhof, M., 1996. Generalized Gradient Approximation Made Simple. *Physical Review Letters* 77(18), 3865-3868.

Perdew, J. P., Chevary, J. A., Vosko, S. H., Jackson, K. A., Pederson M. R., and Fiolhais, C., 1992. Atoms, Molecules, Solids, and Surfaces, Applications of The

Generalized Gradient Approximation for Exchange and Correlation. *Physical Review B* 46 , 6671-6678.

Prasai, B., Cai, B., Underwood, M. K., Lewis, J. P., and Drabold, D. A., 2012. Properties of Amorphous and Crystalline Titanium Dioxide from First Principles. *Journal of Materials Science* 47(21), 7515-7521.

SCM, 2014. *ADF-Band version 2014.10*, Vrije Universiteit, Amsterdam : The Netherlands.

Sutrisno, H., and Sunarto. 2014. *Perhitungan Awal Struktur Pita dan Density of State (DOS) Fasa Anatas dan Rutile dengan Model Struktur Kristal Eksperimen.* Prosiding Seminar Nasional Dies Natalis ke-50 Universitas Negeri Yogyakarta.

Swope, R. J., Smyth, J. R., and Larson, A. C., 1995. H in Rutile-Type Compounds, I. Single-Crystal Neutron and X-Ray Diffraction Study of H in Rutile. *American Mineralogist* 80, 448-453.

Tan, B., and Wu, Y., 2006. Dye-Sensitized Solar Cells Based on Anatase TiO_2 Nanoparticle/Nanowire Composites. *Journal of Physical Chemistry B* 110, 15932-15938.

Tang, H., Prasad K., Sanjinès R., Schmidt P. E., and Lévy F., 1994. Electrical and Optical Properties of TiO_2 Anatase Thin Films. *Journal of Applied Physics* 75, 2042-2047.

Thuy, N. M., Van, D. Q., and Hai, L. T. H., 2012. The Visible Light Activity of The TiO_2 and TiO_2,V^{4+} Photocatalyst. *Nanomaterials and Nanotechnology* 2, 1-8.

Tian, B., Li, C., and Zhang, J., 2012. One Step Preparation, Characterization and Visible-Light Photo-Catalytic Activity of Cr-Doped TiO_2 with Anatase and Rutile Bicrystalline Phases. *Chemical Engineering Journal* 191, 402-409.

Wang, H., Niu, J., Long, X., and He, Y., 2008. Sonophotocatalitic Degradation of Methyl Orange by Nanosized Ag/TiO_2 Particles in Aqueous Solutions. *Ultrasonic Sonochemistry* 15, 386-392.

Wang, Y., Zhang, R., Li, J., Li., L., and Lin, S. 2014. First-Principles Study on Transition Metal-Doped Anatase TiO_2. *Nanoscale Research Letter* 9, 46-54.

Weirich, T. E., Winterer, M., Seifried, S., Hahn, H. and Fuess, H., 2000. Rietveld Analysis of Electron Powder Diffraction Data from Nanocrystalline Anatase TiO_2. *Ultramicroscopy* 81(3-4), 263-270.

Yang, J., Cui, S., Qiao, J. Q., and Lian, H. Z., 2014. The Photocatalytic Dehalogenation of Chlorophenols and Bromophenols by Cobalt Doped Nano TiO_2. *Journal of Molecular Catalysis A: Chemical* 395, 42-51.

Yang, X., Cao, C., Hohn, K., Erickson, L., Maghirang, R., Hamal, D., and Klabunde, K., 2007. Highly Visible Light Active C- and V-Doped TiO_2 for Degradation of Acetaldehyde. *Journal Catalysis* 252, 296-302.

Zhang, D. R., Liu, H. N., Han, S. Y., and Piao, W. X., 2013. Synthesis of Sc- and V-Doped TiO_2 Nano-Particles and Photodegradation of Rhodamine-B. *Journal of Industrial an Engineering Chemistry* 19, 1838-1844.

Zhang, J., Wu, B., Huang, L., Liu, P., Wang, X., Lu, Z., Xu, G., Zhang, E., Wang, H., Kong, Z., Xi, J., and Ji, Z., 2016. Anatase Nano-TiO_2 with Exposed Curved Surface for High Photocatalytic Activity. *Journal of Alloys and Compound* 661, 441-447.

Zhao, K., Wu, Z., Tang, R., and Jiang, Y., 2013. Preparation of Highly Visible-Light Photocatalytic Active N-Doped TiO_2 Microcuboids. *Journal of Korean Chemical Society* 57(4), 489-492.

Zhao, Y., Qiu, X., and Burda, C., 2008. The Effects of Sintering on The Photocatalytic Activity of N-Doped TiO_2 Nanoparticles. *Chemistry of Material* 20, 2629-2636.